

Preparation and characterization of $\text{LaMn}_{0.5}\text{Co}_{0.5}\text{O}_3$ – $\text{Ni}_{0.66}\text{Mn}_{2.34}\text{O}_4$ composite NTC ceramics

Cuiping Huang^{1,2} · Long Chen^{1,2} · Qinan Zhang¹ · Shannan Chang^{1,2} ·
Bo Zhang¹ · Aimin Chang¹ · Huimin Zhang¹

Received: 20 January 2016 / Accepted: 22 March 2016 / Published online: 1 April 2016
© Springer Science+Business Media New York 2016

Abstract Negative temperature coefficient (NTC) thermistor materials based on $(\text{LaMn}_{0.5}\text{Co}_{0.5}\text{O}_3)_x$ – $(\text{Ni}_{0.66}\text{Mn}_{2.34}\text{O}_4)_{1-x}$ ($0 \leq x \leq 0.5$) composite ceramics, are fabricated by the conventional solid-state reaction method. The crystal structure, surface morphology and electrical properties of the composite ceramics are investigated and characterized by X-ray powders diffraction (XRD), scanning electron microscope (SEM), and Agilent digital multimeter, respectively. XRD results show that main phases of as-sintered ceramics are a cubic spinel structure $\text{Ni}_{0.66}\text{Mn}_{2.34}\text{O}_4$ phase and a rhombohedral perovskite structure $\text{LaMn}_{0.5}\text{Co}_{0.5}\text{O}_3$ phase. SEM images indicate that the grain size of the composite ceramics decreases with increasing the low-resistivity perovskite phase. The ρ_{25} and B value of the composite ceramics decreases with increasing x, and the B is still reasonably high in the range of 4000–3500 K when $x \leq 0.2$. Meanwhile, the introduction of the perovskite phase leads to a decrease in the resistance drift, which the $\Delta R/R_0$ is relatively low (0.26–1.8 %) after annealing at 125 °C for 600 h in air atmosphere. These findings exhibit that $(\text{LaMn}_{0.5}\text{Co}_{0.5}\text{O}_3)_x$ – $(\text{Ni}_{0.66}\text{Mn}_{2.34}\text{O}_4)_{1-x}$ ($0 \leq x \leq 0.5$) composite

ceramics have a higher electrical stability in comparison with $\text{Ni}_{0.66}\text{Mn}_{2.34}\text{O}_4$ ceramics, are helpful for meeting demands for obtaining better stability and performance of NTC composites ceramics.

1 Introduction

NTC thermistors are thermally sensitive resistors whose resistance presents exponential decrease with the increasing of the temperature. Because of its various virtues, like high sensitivity, stable resistant, fast response, small volume and low cost, it is widely used for temperature sensors, temperature compensation devices, metallic thermocouples, semi-conductive ceramics, and suppression of in-rush current [1–3]. As a general rule, resistivity and material constant B usually are used to characterize the performance of NTC thermistors [4]. The resistivity is defined as:

$$\rho = \rho_0 \exp(B/T) \quad (1)$$

where the ρ_0 is the resistivity at infinity temperature, T is the absolute temperature, and the material constant B of NTC thermistor is a measure of the equipment sensitivity under a specific temperature [5, 6], which shows the sensitive degree of resistance to the change of temperature [1]. The definition of B is:

$$B = Ea/k \quad (2)$$

where the Ea is the electronic activation energy, and k is the Boltzmann constant.

Generally, the B value is small when the resistivity is low. But sometimes, the condition of application requires the resistivity buck the trend changes to the value of B. Composite is one of the feasible ways to solve this problem by turning compositions and dopants [5, 7–10]. NTC

✉ Aimin Chang
kmkuangyang@126.com; changam@ms.xjb.ac.cn

✉ Huimin Zhang
zhanghm@ms.xjb.ac.cn

¹ Key Laboratory of Functional Materials and Devices for Special Environments of CAS, Xinjiang Key Laboratory of Electronic Information Materials and Devices, Xinjiang Technical Institute of Physics and Chemistry, Chinese Academy of Sciences, 40-1 South Beijing Road, Ürümqi 830011, Xinjiang, China

² University of Chinese Academy of Sciences, Beijing 100049, China

ceramics based on Ni–Mn series with general formula $(\text{Ni}, \text{Mn})_3\text{O}_4$ are one of the most widely used ceramic materials, such as Mn–Co–Ni–O [11–13], Ni–Co–Mn–Fe–O [14], Ni–Mn–Cu–Zn–O [5], Ni–Mn–O [15, 16]. In general, this kind of material follows the law that the resistivity rises as the thermal activation energy increases. While LaMnO_3 is known for its low resistivity, for instance, the electrical resistivity of pure LaMnO_3 is lower than $1 \Omega \text{ cm}$ at room temperature [17]. Therefore, many researchers focus their thought on the composite of La–Mn–O and Ni–Mn–O ceramic systems [9, 18, 19]. Zhao et al. [19] chose the $\text{LaMnO}_3\text{--Ni}_{0.75}\text{Mn}_{2.25}\text{O}_4$ composite as the support layer, $\text{Ni}_{0.75}\text{Mn}_{2.25}\text{O}_4$ as the sensitive layer, and successfully prepared bilayer NTC thermistors. However, there are few researches on the system $\text{LaMn}_{0.5}\text{Co}_{0.5}\text{O}_3\text{--Ni}_{0.66}\text{Mn}_{2.34}\text{O}_4$ composite ceramics. So in this paper, the new series of $\text{LaMn}_{0.5}\text{Co}_{0.5}\text{O}_3\text{--Ni}_{0.66}\text{Mn}_{2.34}\text{O}_4$ composite ceramics were prepared. The effect of perovskite amount on crystal structure, surface morphology thermal stability, and electrical properties of the composite ceramics were investigated.

2 Experimental

The $(\text{LaMn}_{0.5}\text{Co}_{0.5}\text{O}_3)_x\text{--}(\text{Ni}_{0.66}\text{Mn}_{2.34}\text{O}_4)_{1-x}$ samples were prepared by conventional solid-state reaction synthesis method. To prepare $\text{LaMn}_{0.5}\text{Co}_{0.5}\text{O}_3$ and $\text{Ni}_{0.66}\text{Mn}_{2.34}\text{O}_4$ powders, analytical-purity oxide powders MnO_2 , Ni_2O_3 , Co_2O_3 , La_2O_3 were weighed and mixed on the basis of appropriate stoichiometric ratio, as well as deionized water as a dispersant agent and agate balls as grinding media. The mixtures of weighed powders were mixed by ball-milling for 8 h at room temperature using a planetary mill. Then the ball-milled slurries were dried at $80 \text{ }^\circ\text{C}$ for 12 h in a constant temperature drying oven. Subsequently, the dried powders were ground in a mortar and calcined at 1000 and $950 \text{ }^\circ\text{C}$ for 2 h, respectively. Then the expectant pure phase was obtained.

The above-mentioned two kinds of calcined powders were individually ground in mortar for 4 h, and then the composite $(\text{LaMn}_{0.5}\text{Co}_{0.5}\text{O}_3)_x\text{--}(\text{Ni}_{0.66}\text{Mn}_{2.34}\text{O}_4)_{1-x}$ ($0 \leq x \leq 0.5$), where x represents the molar ratios) was produced by mixing desired molar ratios of as-prepared $\text{LaMn}_{0.5}\text{Co}_{0.5}\text{O}_3$ and $\text{Ni}_{0.66}\text{Mn}_{2.34}\text{O}_4$ source powders. The mixtures were then ground for 6 h, respectively. Through the uniaxial pressing and cold isostatic pressing, the mixture powder was compacted into pellets with a diameter of 10 mm. These pressed green compacts were sintered in Clock Hood-type furnace at $1250 \text{ }^\circ\text{C}$ for 4 h in ambient air atmosphere.

The crystalline phases of the calcined powder and sintered pellets were analyzed by X-ray diffraction (XRD; BRUKERD2-ADVANCE, Germany) with $\text{Cu K}\alpha$

radiation. The surface microstructure and phase composition of composite ceramics were characterized by the scanning electron microscope (SEM; LEO 1430VP, Germany), coupling with energy dispersive spectroscopy (EDS). In order to measure the electrical properties of the composite ceramics, the sintered ceramics were spread with a thin silver layer of silver–palladium conductive paste as electrode on both of two opposite sides, and then the pellets with silver-layer were heated at $835 \text{ }^\circ\text{C}$ for 40 min. The resistances of the coated ceramics at different temperature were measured by Agilent34970A digital multimeter bathing in silicon oil range from -80 to $80 \text{ }^\circ\text{C}$. The material constant B values were acquired in accordance with:

$$B = \frac{T_1 \times T_2}{T_2 - T_1} \times \ln\left(\frac{R_1}{R_2}\right) \quad (3)$$

The R_1 and R_2 represents the resistance of the composite ceramics at T_1 and T_2 , respectively.

3 Results and discussion

3.1 Phase composition and microstructure

Figure 1 shows the XRD patterns of $(\text{LaMn}_{0.5}\text{Co}_{0.5}\text{O}_3)_x\text{--}(\text{Ni}_{0.66}\text{Mn}_{2.34}\text{O}_4)_{1-x}$ ($0 \leq x \leq 0.5$) composite ceramics sintered at $1250 \text{ }^\circ\text{C}$. When $x = 0$, the pure $\text{Ni}_{0.66}\text{Mn}_{2.34}\text{O}_4$ was obtained in ceramics, while $x > 0$, it can be seen that the composite ceramics consist of two phases, a cubic spinel phase (JCPDS Card No. 13-0162) and a rhombohedral perovskite phase (JCPDS Card No. 50-0297). What's more, as the x content increased from 0 to 0.3, the main peak of composite ceramics was still the spinel phase.

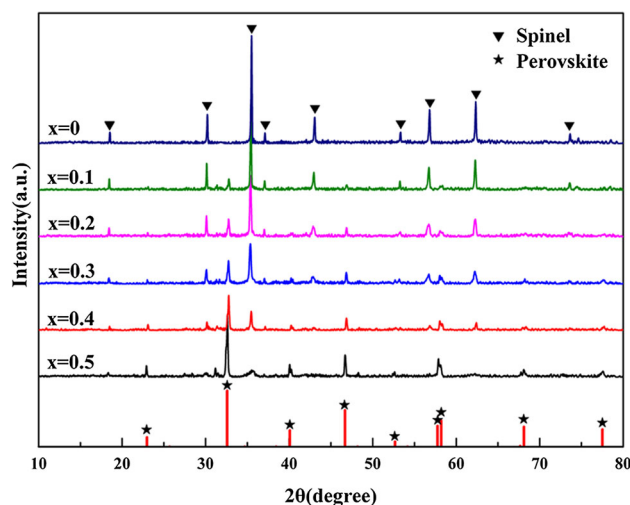


Fig. 1 XRD patterns of $(\text{LaMn}_{0.5}\text{Co}_{0.5}\text{O}_3)_x\text{--}(\text{Ni}_{0.66}\text{Mn}_{2.34}\text{O}_4)_{1-x}$ ($0 \leq x \leq 0.5$) ceramics

When x was larger than 0.3, the main peak of composite ceramics became perovskite phase. From the image, it can be seen that the peaks of spinel phase in the composite ceramics slightly shifted towards higher angles with respect to the $\text{Ni}_{0.66}\text{Mn}_{2.34}\text{O}_4$, indicating that the unit cell volume of spinel phase slightly decreases with the increase of x . As the x content increased the widths of spinel peaks became wider, indicating that the grain size decreases. These results indicate that the introduction of perovskite phases restrains the grain growth of the perovskite phase $\text{LaMn}_{0.5}\text{Co}_{0.5}\text{O}_3$.

Figure 2 shows the backscattered SEM images obtained from the surfaces of the sintered composite ceramics. From the images, we can see the composite ceramics consist of two kinds of grains with different size. It can be observed

that all the oxide ceramics showed well-sintered and well-grown grains, and highly dense. What's more, the microstructure of the spinel phase was strongly dependent on the introduction of perovskite phase $\text{LaMn}_{0.5}\text{Co}_{0.5}\text{O}_3$. The average grain size obviously decreased as the introduced perovskite content increased, which indicates that the grain growth is restrained by the presence of the perovskite phase $\text{LaMn}_{0.5}\text{Co}_{0.5}\text{O}_3$. This result is corresponding to XRD result. In addition, it can be found that the grain size of the perovskite phase was still smaller than the spinel phase.

In order to identify the distribution of constituent elements in the composite ceramics, Fig. 3 is given, which shows the distribution of different elements. Different color represents for diverse elements, especially, green for La

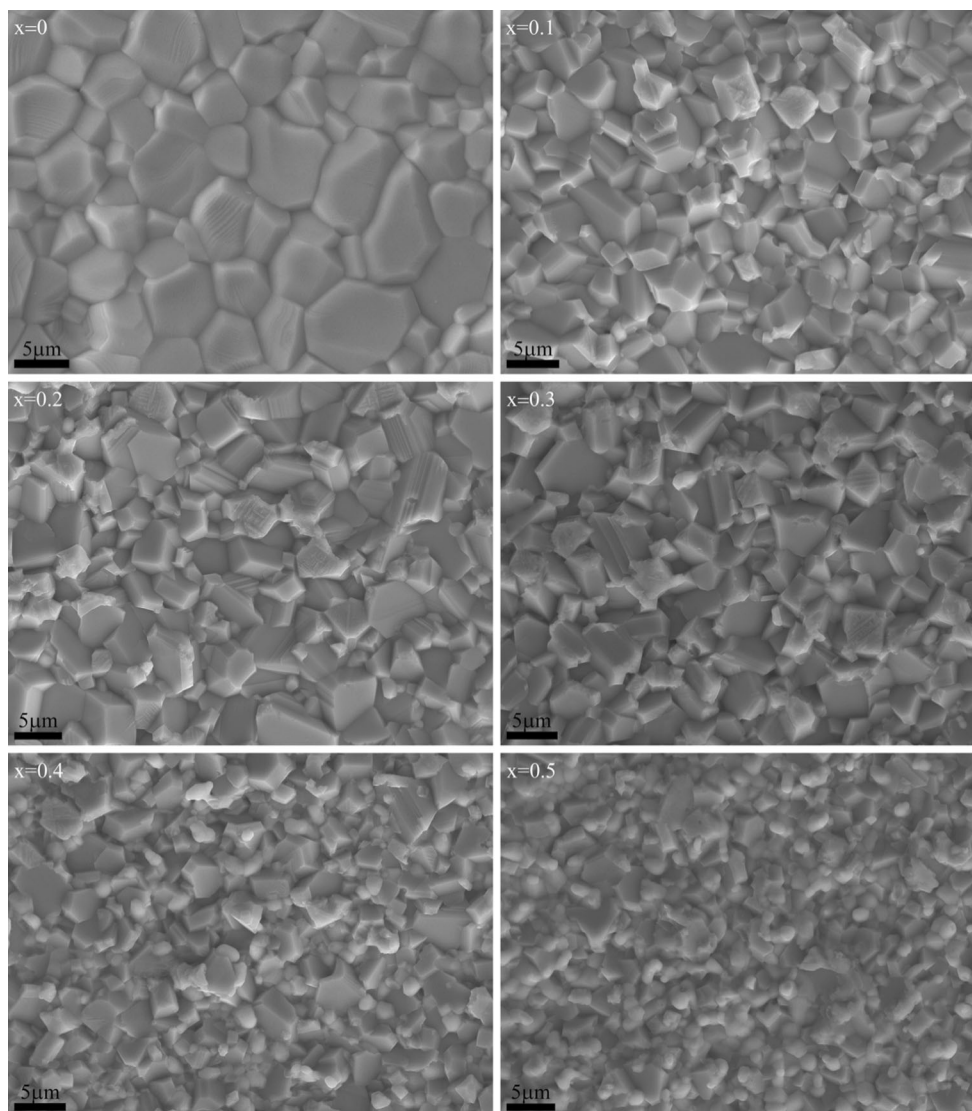


Fig. 2 SEM images of $(\text{LaMn}_{0.5}\text{Co}_{0.5}\text{O}_3)_x(\text{Ni}_{0.66}\text{Mn}_{2.34}\text{O}_4)_{1-x}$ ($0 \leq x \leq 0.5$) ceramics

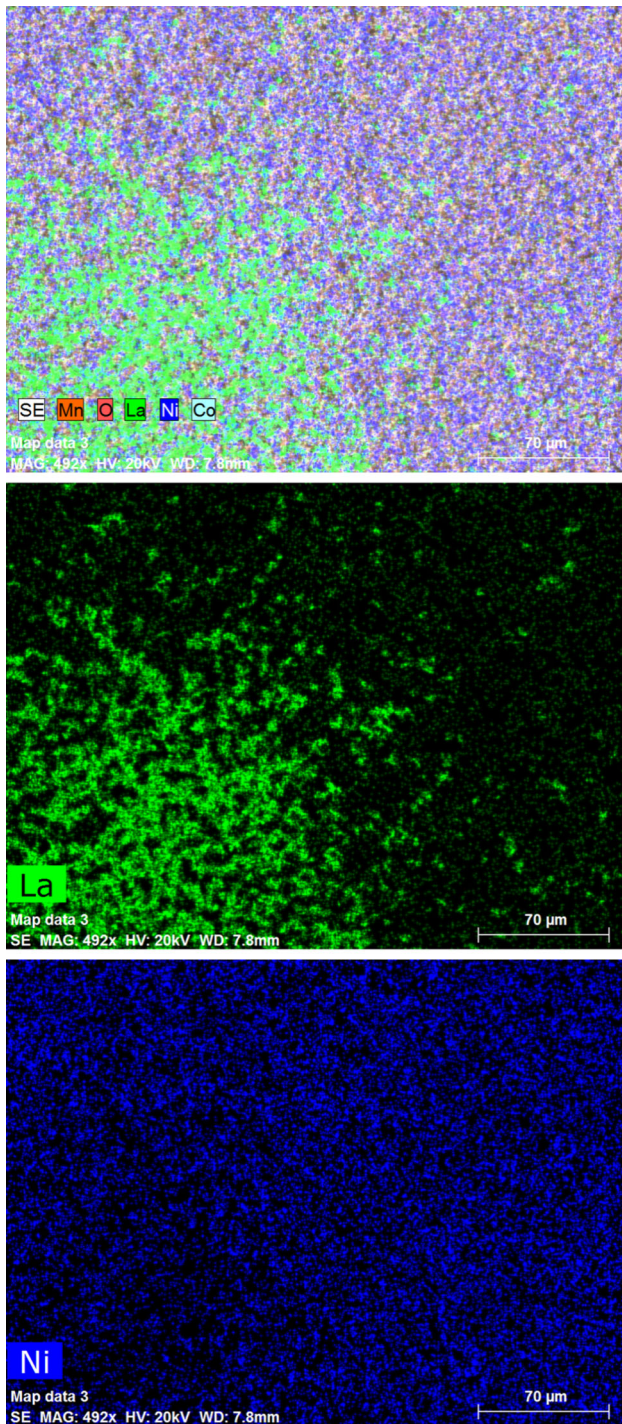


Fig. 3 EDS images of $(\text{LaMn}_{0.5}\text{Co}_{0.5}\text{O}_3)_{0.4}(\text{Ni}_{0.66}\text{Mn}_{2.34}\text{O}_4)_{0.6}$ ceramics (Color figure online)

and blue for Ni. Since La is only in the $\text{LaMn}_{0.5}\text{Co}_{0.5}\text{O}_3$, while Ni only in $\text{Ni}_{0.66}\text{Mn}_{2.34}\text{O}_4$, it is believed that green represents perovskite phase, and blue represents spinel phase, indicating that two different phases in composite structure. The result is accordance with the XRD result.

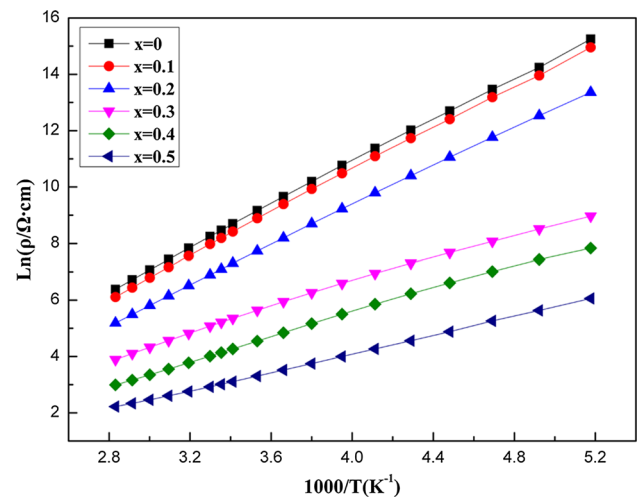


Fig. 4 Arrhenius plot of resistivity for $(\text{LaMn}_{0.5}\text{Co}_{0.5}\text{O}_3)_x(\text{Ni}_{0.66}\text{Mn}_{2.34}\text{O}_4)_{1-x}$ ($0 \leq x \leq 0.5$) ceramics

3.2 Electrical properties

Figure 4 exhibits the relationship between the $\ln \rho$ and reciprocal of the absolute temperature. It can be directly seen that a linear relationship was obtained with increasing x content from 0 to 0.5. In addition, the resistivity of the composite decreases gradually with increasing temperature, which means the composites exhibit a typical NTC thermistor characteristics. From the picture, we can see that the room-resistivity of the composite ceramics decreases as the x increases from 0 to 0.5. The percolation models consider that introducing a conductive material into an insulating material will increase the conductivity of the mixtures [20]. So the resistivity decrease of composite ceramics can be attributed to the introduction of the low-resistivity perovskite phase $\text{LaMn}_{0.5}\text{Co}_{0.5}\text{O}_3$. Meanwhile, the carrier concentration and mobility determine the electrical conduction of the composite. It is commonly believed that the conductive mechanism of spinel structure NTC ceramics is due to the hopping process between the metal ions, such as Mn^{3+} , Mn^{4+} [13, 21, 22]. The introduction of perovskite $\text{LaMn}_{0.5}\text{Co}_{0.5}\text{O}_3$ results in an increase of the ion pairs of $\text{Mn}^{3+}/\text{Mn}^{4+}$, which are important to the electrical conductivity of Mn-based NTC thermistors [23]. The increase of $\text{Mn}^{3+}/\text{Mn}^{4+}$ will augment the carrier concentration, lower the energy barriers for polaron hopping and increase the tendency to form small polarons, thus decreasing the resistivity of composite ceramics.

The room-temperature resistivity (ρ_{25}), the material constant determining the temperature sensitivity of the NTC thermistor ($B_{25/50}$), as a function of x are depicted in Fig. 5. It can be observed that the ρ_{25} and B value decrease with increasing x from 0 to 0.5. The resistivity at 25 °C (ρ_{25}), material constant ($B_{25/50}$), temperature coefficient of

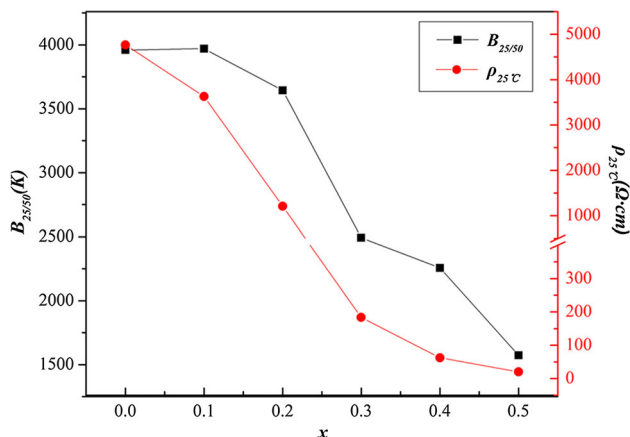


Fig. 5 The room-temperature resistivity ρ_{25} and material constant $B_{25/50}$ of $(\text{LaMn}_{0.5}\text{Co}_{0.5}\text{O}_3)_x(\text{Ni}_{0.66}\text{Mn}_{2.34}\text{O}_4)_{1-x}$ ($0 \leq x \leq 0.5$) ceramics

Table 1 Resistivity, B constant, activation energy, and temperature coefficient of resistance (α_{25}) for the composite ceramics

| X | ρ_{25} (Ω cm) | $B_{25/50}$ (K) | E_a (eV) | α_{25} (%/K) |
|-----|----------------------------|-----------------|------------|---------------------|
| 0 | 4767 | 3960 | 0.3416 | -4.4593 |
| 0.1 | 3628 | 3970 | 0.3424 | -4.4705 |
| 0.2 | 1207 | 3643 | 0.3142 | -4.1023 |
| 0.3 | 183 | 2492 | 0.2149 | -2.8062 |
| 0.4 | 63 | 2257 | 0.1947 | -2.5416 |
| 0.5 | 20 | 1573 | 0.1357 | -1.7713 |

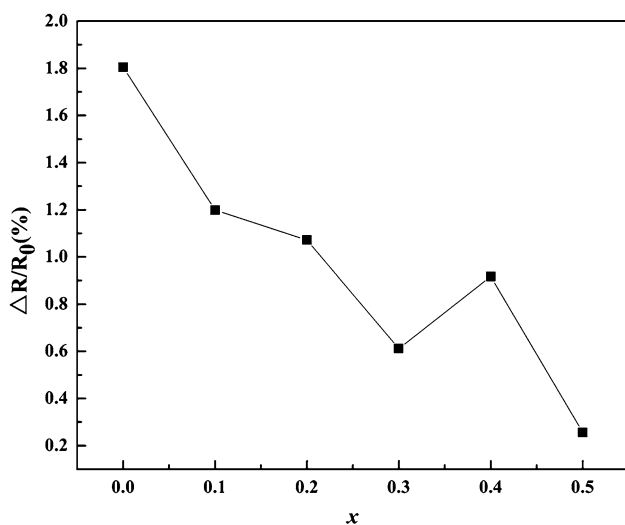


Fig. 6 The relative resistance drift of $(\text{LaMn}_{0.5}\text{Co}_{0.5}\text{O}_3)_x(\text{Ni}_{0.66}\text{Mn}_{2.34}\text{O}_4)_{1-x}$ ($0 \leq x \leq 0.5$) ceramics after aging test at 125 °C for 600 h in air atmosphere

resistance (α_{25}) and activation energy (E_a) for composite ceramic samples are listed in Table 1 to illustrated the electrical properties variation exactly. As shown in

Table 1, the values of ρ_{25} , $B_{25/50}$, E_a , and α_{25} for the composite ceramic samples at different sintering temperatures are the range of 4767–20 Ω cm, 3970–1573 K, 0.3424–0.1357 eV, and -4.4705 to -1.7713 %, respectively. These results indicate that the electrical properties of the composite ceramics can be adjusted by changing $\text{LaMn}_{0.5}\text{Co}_{0.5}\text{O}_3$ content.

Figure 6 exhibits the relative resistance drift ($\Delta R/R_0$) for the composites after aging test at 125 °C for 600 h in air atmosphere. It can be seen that the values of $\Delta R/R_0$ decreases from apparently with the increasing of x . The $\Delta R/R_0$ was within the scope of 1.20–0.26 % with increasing x content from 0.1 to 0.5, which is smaller than that 1.8 % for the single $\text{Ni}_{0.66}\text{Mn}_{2.34}\text{O}_4$ ceramics. It indicates that appropriate introduction of $\text{LaMn}_{0.5}\text{Co}_{0.5}\text{O}_3$ can improve the material stability, it is likely that the presence of perovskite prevodes a physical barrier to the aging of composite [18]. This composite ceramics can be apply into high stability NTC thermistor application.

4 Conclusion

The composite ceramic $(\text{LaMn}_{0.5}\text{Co}_{0.5}\text{O}_3)_x(\text{Ni}_{0.66}\text{Mn}_{2.34}\text{O}_4)_{1-x}$ ($0 \leq x \leq 0.5$) prepared by classical solid-state method, consists of two structures of spinel-structured oxide $\text{Ni}_{0.66}\text{Mn}_{2.34}\text{O}_4$ and perovskite-structured oxide $\text{LaMn}_{0.5}\text{Co}_{0.5}\text{O}_3$. The introduction of low-resistivity perovskite oxide $\text{LaMn}_{0.5}\text{Co}_{0.5}\text{O}_3$ causes a change of phase structure and a decrease of the grain size. In addition, the microstructure and electrical properties of NTC composite ceramics can be tuned as the complex amount changes. The values of ρ_{25} , $B_{25/50}$, E_a , and α_{25} for the composite ceramic samples at different sintering temperatures are the range of 4767–20 Ω cm, 3970–1573 K, 0.3424–0.1357 eV, and -4.4705 to -1.7713 %, respectively. Composite ceramic materials with low resistivity, high material constant B and good stability, are achieved when x is 0.2. These composites, exhibiting good NTC characteristic and high performance, could be applied as potential candidates for NTC thermistor applications.

Acknowledgments This work is supported by the Xinjiang Urgur Autonomous Region Science and Technology Program of China (No. 201554139).

References

1. S. Fritsch, J. Sarrias, M. Brieu, J.J. Couderc, J.L. Baudour, E. Snoeck, A. Rousset, Solid State Ion **109**, 229 (1998)
2. J. Huang, Y.D. Hao, H. Lin, D.L. Zhang, J.J. Song, D.X. Zhou, Mater. Sci. Eng. B **99**, 523 (2003)
3. A. Feteira, J. Am. Ceram. Soc. **92**, 967 (2009)
4. K. Park, J.K. Lee, J. Alloys Compd. **475**, 513 (2009)

5. C.H. Zhao, B.Y. Wang, P.H. Yang, L. Winnubst, C.S. Chen, J. Eur. Ceram. Soc. **28**, 35 (2008)
6. K. Park, I.H. Han, J. Electroceram. **17**, 1069 (2006)
7. K. Park, J.K. Lee, Scr. Mater. **57**, 329 (2007)
8. J.E. Kang, J. Ryu, G. Han, J.J. Choi, W.H. Yoon, B.D. Hahn, J.W. Kim, C.W. Ahn, J.H. Choi, D.S. Park, J. Alloys Compd. **534**, 70–73 (2012)
9. C.H. Zhao, Z.B. Wang, S.M. Wang, P.H. Yang, C.S. Chen, J. Electroceram. **20**, 113 (2008)
10. C.L. Yuan, T. Yang, Y. Luo, C.R. Zhou, G.H. Chen, Y. Yang, J. Mater. Sci. Mater. Electron. **25**, 3967 (2014)
11. L. Chen, W.W. Kong, J.C. Yao, H.M. Zhang, B. Gao, Y.L. Li, H.J. Bu, A.M. Chang, C.P. Jiang, Ceram. Int. **41**, 2847 (2015)
12. W.M. Wang, X.C. Liu, F. Gao, C.S. Tian, Ceram. Int. **33**, 459 (2007)
13. S.A. Kanade, V. Puri, Mater. Lett. **60**, 1428 (2006)
14. H.M. Zhang, A.M. Chang, C.W. Peng, Microelectron. Eng. **88**, 2934 (2011)
15. D.L. Fang, Z.B. Wang, P.H. Yang, W. Liu, C.S. Chen, A.J.A. Winnubst, J. Am. Ceram. Soc. **89**, 230 (2006)
16. C. Ma, Y. Liu, Y. Lu, J. Mater. Sci. Mater. Electron. **26**, 7238–7243 (2015)
17. I. Maurin, P. Barboux, Y. Lassailly, J.P. Boilot, F. Villain, P. Dordor, J. Solid State Chem. **160**, 123 (2001)
18. F. Guan, H.M. Zhang, A.M. Chang, P.J. Zhao, B. Zhang, J. Mater. Sci. Mater. Electron. **23**, 1728 (2012)
19. Y.L. Zhao, C.H. Zhao, J. Huang, B. Zhao, J. Am. Ceram. Soc. **97**, 1016 (2014)
20. F. Lux, J. Mater. Sci. **28**, 285 (1993)
21. K. Park, I.H. Han, J. Electroceram. **17**, 1079 (2006)
22. K. Park, J. Am. Ceram. Soc. **88**, 862 (2005)
23. F. Cheng, J. Wang, H. Zhang, A. Chang, W. Kong, B. Zhang, L. Chen, J. Mater. Sci. Mater. Electron. **26**, 1374–1380 (2015)